ARTICLE

Photocatalytic Activity of N-doped TiO_2 Photocatalysts Prepared from the Molecular Precursor $(NH_4)_2TiO(C_2O_4)_2$

Jing Bu, Jun Fang, Fu-cheng Shi, Zhi-quan Jiang, Wei-xin Huang*

Hefei National Laboratory for Physical Sciences at the Microscale, CAS Key Laboratory of Materials for Energy Conversion, Department of Chemical Physics, University of Science and Technology of China, Hefei 230026, China

(Dated: Received on November 24, 2009; Accepted on December 25, 2009)

We developed a novel approach for the preparation of N-doped TiO_2 photocatalysts by calcining ammonium titanium oxalate at different temperatures. The structures of N-TiO_2 were characterized by powder X-ray diffraction, infrared spectroscopy, thermogravimetric analysis, N_2 adsorption-desorption isotherms, X-ray photoelectron spectroscopy, diffuse reflectance UV-Vis spectroscopy, and scanning electron microscope. The N-doped TiO_2 photocatalysts calcined below 700 °C are the pure anatase phase but that calcined at 700 °C is a mixture of anatase and rutile phases. The doped N locates at the interstitial site of TiO_2 which leads to the narrowing of bad gap of pure anatase N-TiO_2. Among all photocatalysts, N-TiO_2 photocatalysts calcined at 600 and 400 °C exhibit the best performance in the photodegradation of methyl orange under the UV light and all-wavelength light illuminations, respectively; however, because of the perfect crystallinity and the existence of anatase-rutile phase junctions, N-TiO_2 photocatalyst calcined at 700 °C exhibits the highest specific photodegradation rate, *i.e.*, the highest quantum yield, under both the UV light and all-wavelength light illuminations.

Key words: N-doped TiO_2, Ammonium titanyl oxalate, Photocatalysis

I. INTRODUCTION

Titanium dioxide (TiO_2), as a low cost, nontoxic, long-term stability photocatalyst, is one of the most promising materials for many photochemical applications such as the photocatalytic degradation of organic pollutants, the purification of the air, the splitting of water for the H_2 production, *etc.* [1−3]. However, because of the wide band gap of TiO_2 (3.2 eV for anatase), only a small UV fraction of solar light (3%−5%) can be utilized when TiO_2 is used as the photocatalyst. Therefore, great efforts have been devoted to the preparation of efficient TiO_2 photocatalysts responsive to the visible light.

A promising approach to expand the optical response of TiO_2 to the vislble light spectrum range is to modify TiO_2 with non-metals, such as N [4], S [5], F [6], B [7], I [8], and C [9]. Since the pioneer work of Asahi *et al.* that some substitutional N in the TiO_2 lattice could lead to the photocatalytic activity of the N-TiO_2 under visible light illumination [4], the N-doped TiO_2 has received great interests. Many methods have been developed to prepare visible-light-active N-doped TiO_2, such as sputtering [4, 10, 11], ion implantation [12−14], spray pyrolysis [15], controlled hydrolysis or sol-gel [16−18], and chemical treatment of bare TiO_2 [4, 19]. The N-doped TiO_2 photocatalysts prepared by different methods exhibit some different properties. Asahi *et al.* attributed the visible-light activity of N-doped TiO_2 film prepared by the sputtering method to the narrowing of the bad gap of TiO_2 by the mixing of substitutional N2p states with O2p states [4]. Irie *et al.* prepared the substitutional N-doped TiO_2 by calcining the anatase TiO_2 powder in NH_3 and proposed the formation of an isolated N2p narrow band above the O2p valence band which is responsible for the response to the visible light [20]. Diwald *et al.* found that treating the anatase $TiO_2(110)$ single crystal in a NH_3 flow at 870 K could introduce N species to the interstitial sites of TiO_2 and that the interstitial N species could also narrow the band gap of TiO_2 [21]. Burda *et al.* developed a direct amination method to synthesize $TiO_{2-x}N_x$ at room temperature whose maximum N doping content could reach 8% [22]. Ihara *et al.* proposed O vacancies formed at the grain boundary of N-doped TiO_2 to be responsible for the visible-light activity for the degradation of the acetone [23].

In our previous work [24], we reported the synthesis of mesoporous N-doped TiO_2 by the precipitation of titanyl oxalate complex $[TiO(C_2O_4)_2]^{2-}$ with ammonium hydroxide at a low temperature followed by

*Author to whom correspondence should be addressed. E-mail: huangwx@ustc.edu.cn, Tel.: +86-551-3600435, FAX: +86-551-3600437

the calcination at different temperature. The precursor of N-doped TiO_2 consisted of $Ti(OH)_4$, $TiOC_2O_4$ and crystalline $(NH_4)_2C_2O_4$, and all N-doped TiO_2 photocatalysts exhibited nice photocatalytic activity for the degradation of methyl orange degradation under both UV and all wavelength light illuminations. On basis of these results, we consider that N-doped TiO_2 photocatalysts might be directly prepared by the controlled thermal decomposition of pure ammonium titanium oxalate ($(NH_4)_2TiO(C_2O_4)_2$, ATO).

In this paper, we report the successfully preparation of N-doped TiO_2 by the controlled thermal decomposition of ATO. The structures and photocatalytic activities of N-doped TiO_2 have been investigated in detail.

II. EXPERIMENTS

A. Catalyst preparation

Three solutions were firstly made including 6.806 g titanium tertabutoxide in 40 mL ethanol, 2.521 g oxalic acid in 70 mL ethanol containing 0.72 mL distilled water, and 2.842 g ammonium oxalate in 70 mL distilled water. Then the titanium tertabutoxide solution was added to oxalic acid solution under continuous stirring, forming a white precipitate ($TiOC_2O_4$). Then the ammonium oxalate solution and 210 mL distilled water were added to the solution containing the $TiOC_2O_4$ precipitate. After the vigorous stirring, the $TiOC_2O_4$ precipitate was observed to dissolve gradually and eventually a clear solution formed. The clear solution was evaporated at 70 °C and the white ATO powder was obtained.

The N-doped TiO_2 photocatalysts were prepared by calcining ATO at different temperatures (T) in air for 2 h. The obtained catalysts were denoted as N-TiO_2-T, for example, N-TiO_2-400 denotes the N-doped TiO_2 photocatalyst by calcining ATO at 400 °C in air for 2 h.

B. Catalyst characterizations

Thermogravimetric analysis (TGA) was performed on a Shimadzu TGA50 DTA50 analyzer with a heating rate of 10 °C/min in an air flow. Powder X-ray diffraction (XRD) patterns were recorded on a Philips X'Pert PROS diffractometer using a nickel-filtered Cu Kα (0.15418 nm) radiation source with the operation voltage and operation current being 40 kV and 50 mA, respectively. Microscopic experiments were performed on X-650 scanning electron microscope. N_2 adsorption-desorption isotherms were measured on a Micromeritics ASAP 2020 M^+C system. The sample was degassed at 473 K in N_2 for 4 h prior to the measurement. The pore size distribution of mesoporoes in the samples was analyzed with the BJH method. Infrared spectra were measured with a MAGNA-IR 750 fourier transformed infrared spectrometer capable of measuring the far-infrared spectrum. Diffuse reflectance UV-vis spectra were acquired on a DUV-3700 DUV-Vis-NIR recording spectrophotometer. X-ray photoelectron spectroscopy (XPS) measurements were performed on an ESCALAB 250 high-performance electron spectrometer with monochromatized Al Kα ($h\nu$=1486.7 eV) as the excitation source. The likely charging of samples was corrected by setting the binding energy of the adventitious carbon (C1s) to 284.5 eV.

C. Photocatalytic activity measurements

0.1 g photocatalyst was added to 80 mL methyl orange solution (methyl orange concentration: 20 mg/L). The suspension was stirred in dark for 1 h to reach the adsorption equilibrium and then illuminated by the lamp. Two kinds of 8 W lamps were used: one was a UV lamp with wavelength ranging from 320 nm to 400 nm and the maximum intensity at 365 nm, the other was an all-wavelength light lamp with the wavelength ranging from 380 nm to 700 nm that simulated the sun light spectrum. About 4 mL of the suspension was collected every 2 h and centrifuged. The concentration of methyl orange in the centrifuged aqueous solution was determined by measuring the absorption spectrum of methyl orange at 464 nm on a Shimadzu UV-2450 UV-Visible photometer, from which the photocatalytic activity was evaluated.

III. RESULTS AND DISCUSSION

The synthesis of ATO was previously reported to follow these reactions [25, 26]:

$$Ti(C_4H_9O)_4 + 4H_2O \rightarrow Ti(OH)_4 + 4C_4H_9OH \quad (1)$$

$$Ti(OH)_4 \rightarrow TiO(OH)_2 + H_2O \quad (2)$$

$$TiO(OH)_2 + H_2C_2O_4 \rightarrow TiOC_2O_4 + 2H_2O \quad (3)$$

$$TiOC_2O_4 + (NH_4)_2C_2O_4 \leftrightarrow (NH_4)_2TiO(C_2O_4)_2 \quad (4)$$

The XRD pattern of the catalyst precursor (Fig.1) can be well indexed to that of ATO (PDF No.481165). The IR spectrum of the catalyst precursor (Fig.2) displays the vibrational bands at 765, 1250, 1400, 1690, 1720, 3130, and 3450 cm^{-1}. The two broad bands centering at 3450 and 3130 cm^{-1} could be assigned to the stretch vibration of O−H and N−H, respectively; the bands at 1690 and 1400 cm^{-1} could be assigned to the band vibration of O−H and N−H, respectively. The bands at 1720 and 1250 cm^{-1} arise from different modes of vibration characteristic of the oxalate group. The band at 765 cm^{-1} corresponds to the Ti−O stretch vibration. Therefore, the XRD and IR results confirm the successful preparation of ATO precursor.

Figure 3 shows the TGA and DTG spectra of ATO in an air flow. The TGA curve shows three weight loss steps. The first step between 25 and 180 °C corresponds

DOI:10.1088/1674-0068/23/01/95-101

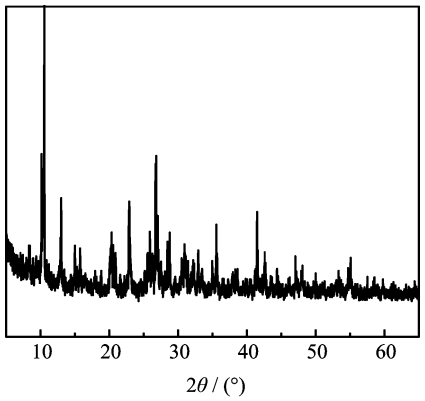

FIG. 1 XRD pattern of ATO.

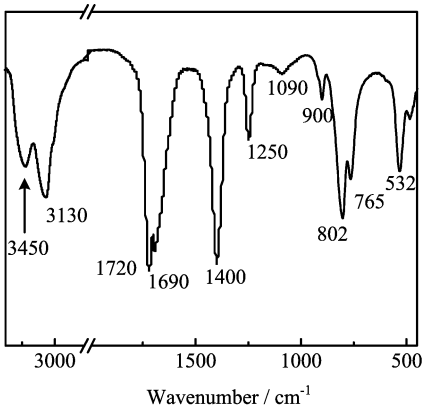

FIG. 2 Infrared spectra of ATO.

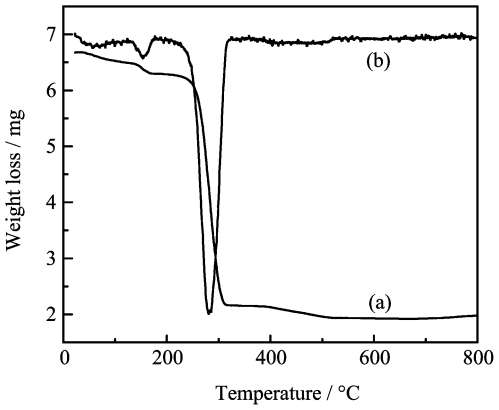

FIG. 3 The TGA (a) and the DTG (b) of ATO in an air flow. The heating rate is 10 °C/min.

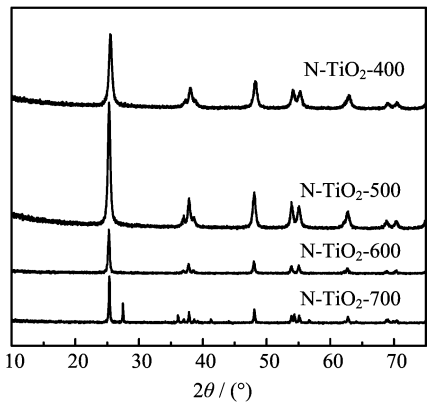

FIG. 4 XRD patterns of the prepared N-doped TiO_2 catalysts.

to the removal of hydrated/adsorbed water and alcohol, and the main weight loss occurs between 180 and 340 °C that could be assigned to the decomposition/oxidation of oxalate and NH_4^+, and the third step above 400 °C might be assigned to the oxidation of carbon formed during decomposition of oxalate. The total weight loss was measured to be 71.18% in TGA, close to the theoretical value (71%) for the decomposition of ATO to TiO_2.

On basis of the TGA results, the following calcination temperatures were chosen for the preparation of TiO_2 from ATO: 400, 500, 600, 700, and 800 °C. Figure 4 displays the XRD patterns of these TiO_2 samples. N-TiO_2-400, N-TiO_2-500, N-TiO_2-600 show the typical pattern of anatase TiO_2, but N-TiO_2-700 shows the XRD patterns of both anatase and rutile TiO_2, and the XRD pattern of N-TiO_2-800 (not shown) is a pure diffraction pattern of rutile TiO_2. There results demonstrate that the phase transformation occurs at ∼700 °C for TiO_2 prepared from the thermal decomposition of ATO. The average crystallite size of anatase TiO_2 was calculated from the Debye-Scherrer equation and the results are summarized in Table I. It can be seen that the average crystallite size of anatase TiO_2 increases from

TABLE I Structural parameters of N-doped TiO_2 catalysts.

Photocatalysts	S_{BET} /(m^2/g)	Pore volume /(cm^3/g)	Pore size /Å	d_{XRD}[a] /nm
N-TiO_2-400	86	0.200	67	15.5
N-TiO_2-500	50	0.164	90	18.9
N-TiO_2-600	29	0.157	157	30.6
N-TiO_2-700	10	0.094	273	50.5

[a] Anatase.

15.2 nm in N-TiO_2-400 to 50.6 nm in N-TiO_2-700. The SEM results (Fig.5) also demonstrate the agglomeration of TiO_2 nanoparticles at the elevated calcination temperatures.

Figure 6(a) shows the N_2 adsorption-desorption isotherms of TiO_2 photocatalysts that are the typical type IV pattern, indicating that the prepared TiO_2 are mesoporous materials. The hysteresis loop in the isotherms is type H_2, according to the IUPAC classification, which could be usually observed in the pores with narrow necks and wide bodies (ink-bottle pores)

DOI:10.1088/1674-0068/23/01/95-101

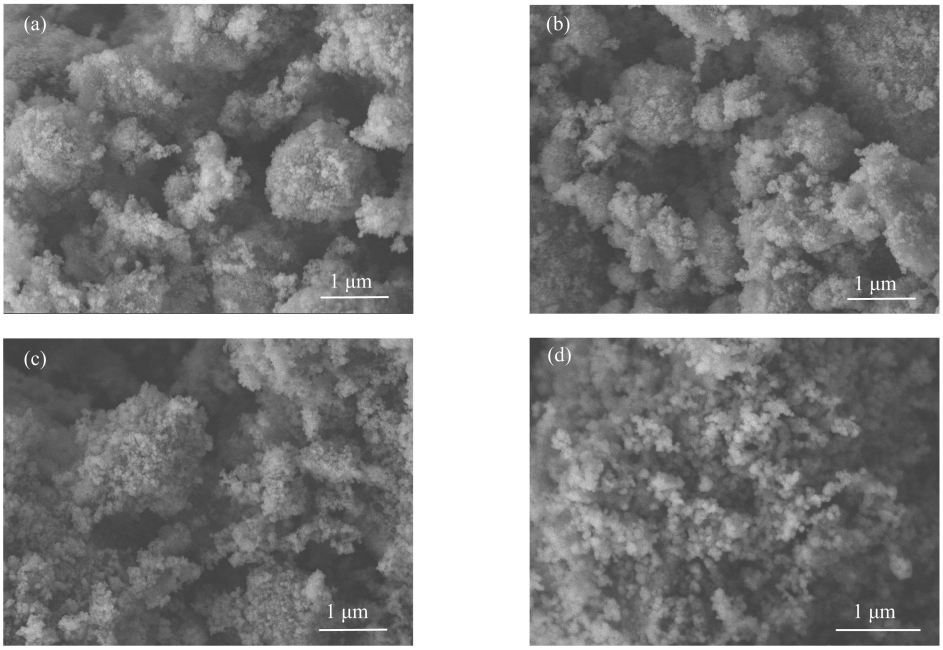

FIG. 5 The scanning electron microscope photographs of the N-doped TiO_2. (a) N-TiO_2-400, (b) N-TiO_2-500, (c) N-TiO_2-600, (d) N-TiO_2-700.

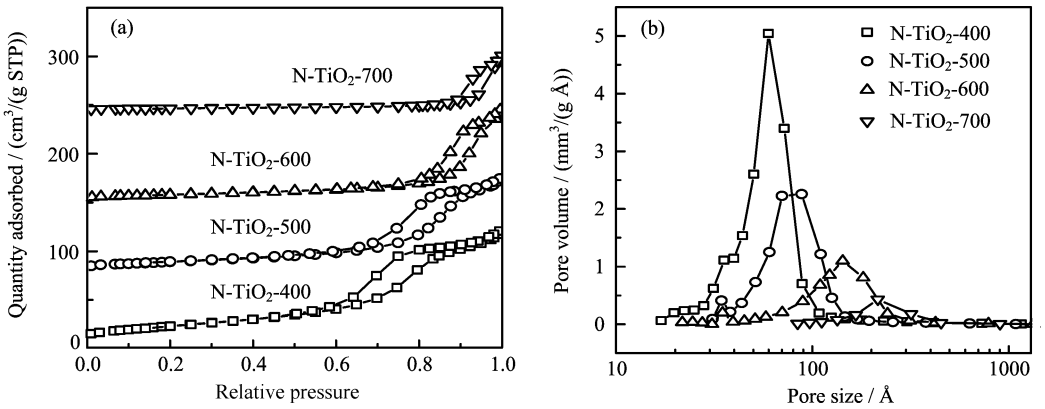

FIG. 6 (a) The N_2 adsorption-desorption isotherms of N-doped TiO_2 catalysts. (b) The size distributions of N-doped TiO_2 catalysts.

[27]. The area of the hysteresis loop in the isotherm of different samples decreases with the increasing of the calcination temperature, indicating the shrinking pore volume. The pore size distributions of various samples (Fig.6(b)) were analyzed with the BJH method from the desorption branch of the isotherms. All the photocatalysts exhibit the monomodal mesoporous size distribution, and as the calcination temperature increases, the pore volume decreases whereas the pore size increases. The BET surface area, the pore volume, and the average pore size of various TiO_2 samples are also summarized in Table I.

The surface compositions of TiO_2 samples were characterized by XPS (Fig.7). The Ti2p XPS spectra show a single component with the $Ti2p_{2/3}$ binding energy at 458.4 eV, corresponding to Ti^{4+} in TiO_2 [28]. The O1s XPS spectra exhibit two components: the major one centered at 529.6 eV corresponding to lattice oxygen in TiO_2 and the other centered at 531.0 eV assigned to surface hydroxyls [28]. The C1s XPS spectra consist of three components with the binding energy at 284.5, 285.9, and 288.3 eV which could be assigned to the adventitious carbon, carbon connected with OH group, and carbonates on the surface of the sample, respectively [28]. The XPS results clearly ruled out the existence of the doped C species in TiO_2 because its binding energy is located at a relative low position 282 eV [29].

All TiO_2 samples exhibit a single N1s XPS peak with at 399.5 eV. The assignment of the N1s XPS peak in the N-doped TiO_2 has been reported by many research

DOI:10.1088/1674-0068/23/01/95-101

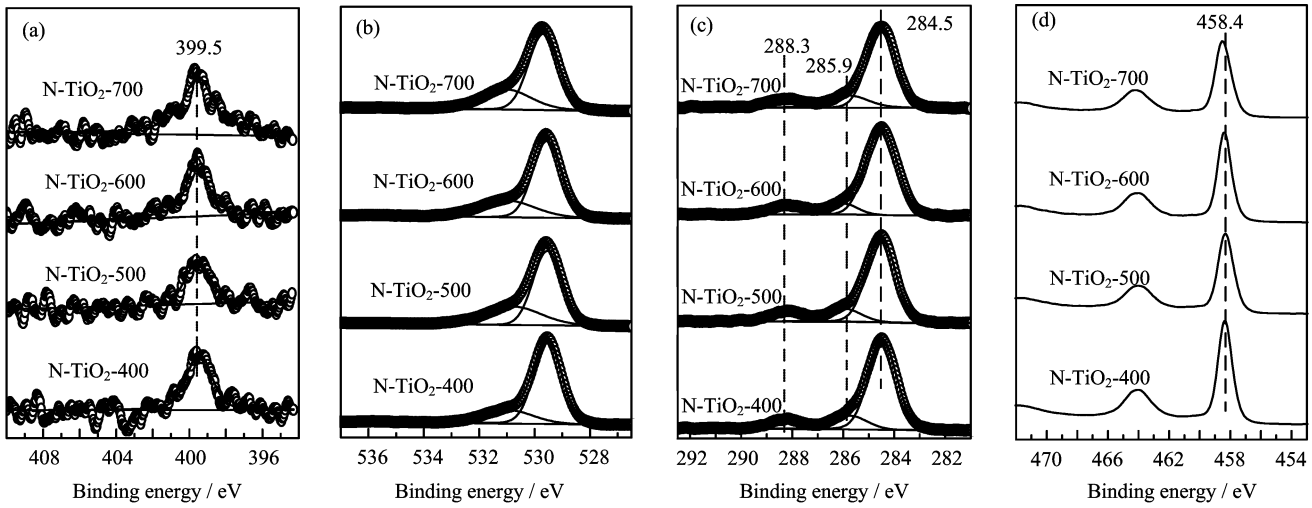

FIG. 7 The N1s (a), O1s (b), C1s (c), Ti2p (d) XPS spectra of N-doped TiO_2 catalysts.

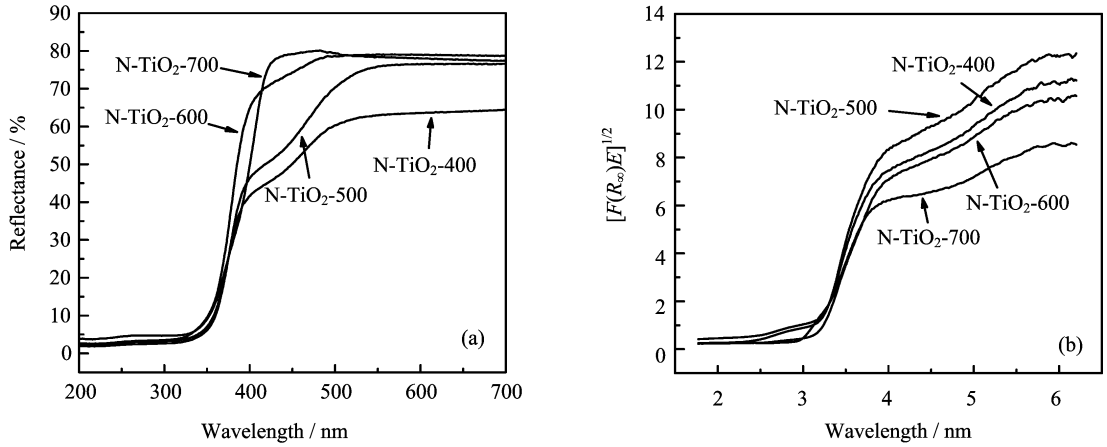

FIG. 8 Diffuse reflectance UV-Vis spectra (a) and transformed diffuse reflectance UV-Vis spectra (b) of N-doped TiO_2 catalysts.

groups. The N^{2-} substituting lattice O in the TiO_2 usually gives a N1s binding energy lattice at 396 eV [30]. Chen *et al.* assigned the N1s peak at 401.3 eV to the O−Ti−N structure during the substitutional doping process and Wang *et al.* assigned the peak at 399.6 eV to the nitrogen atoms in the environment of O−Ti−N linkages [31, 32]. Diward *et al.* prepared N-doped rutile $TiO_2(110)$ by heating in NH_3 and observed two N1s peaks at 396.7 and 399.6 eV. The peak at 399.6 eV was assigned to N atoms located at the interstitial site in rutile, and the nitrogen state was responsible for the red shift of the photochemical threshold of rutile $TiO_2(110)$ down to 2.4 eV [21]. In our previous work [24], we have prepared the anatase TiO_2 doped with N at the interstitial site whose N1s binding energy appeared at 399.6 eV. Therefore, we assign the N1s feature at 399.5 eV to the N species at the interstitial site of TiO_2, clearly demonstrating that TiO_2 photocatalysts prepared from the thermal decomposition of ATO are N-doped. Evaluated from the XPS results, the content of doped N is 0.37%, 0.25%, 0.37%, and 0.37% in N-TiO_2-400, N-TiO_2-500, N-TiO_2-600, and N-TiO_2-700, respectively.

Figure 8(a) shows the UV-Vis diffuse reflectance spectra of the N-doped TiO_2 photocatalysts. All photocatalysts except N-TiO_2-700 demonstrate significant absorption in the visible light region between 400 and 550 nm, a typical absorption region for nitrogen-doped TiO_2 materials. The plots of the modified Kubelka-Munk function $[F(R_\infty)E]^{1/2}$ *vs.* the energy of absorbed light E [17] (Fig.8(b)) demonstrate that the band gap of N-TiO_2-400, N-TiO_2-500, N-TiO_2-600, and N-TiO_2-700 is 3.0, 3.1, 3.1, and 3.0 eV, respectively. The band gap of anatase TiO_2 is 3.2 eV, therefore, N-TiO_2-400, N-TiO_2-500, and N-TiO_2-600 show more or less the narrowing of band gap that could be reasonably attributed to the doped N. Since N-TiO_2-700 is a mixture of anatase and rutile TiO_2 and the band gap of rutile TiO_2 is 3.0 eV,

DOI:10.1088/1674-0068/23/01/95-101

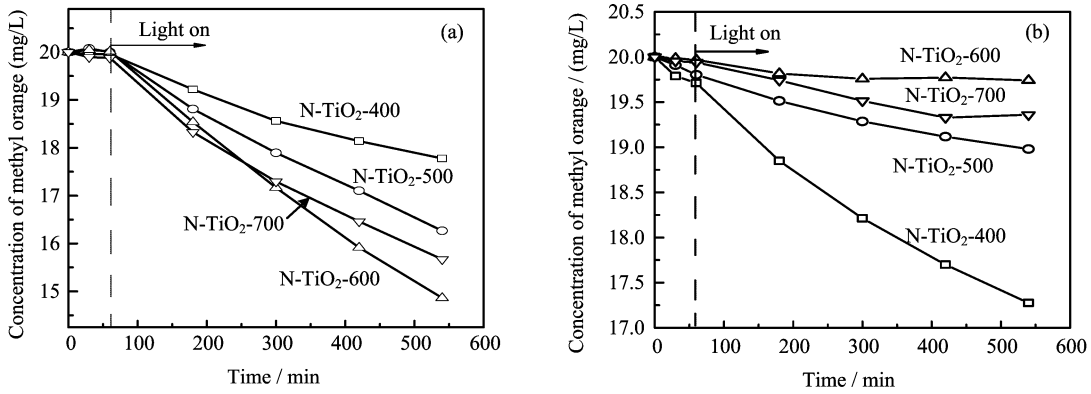

FIG. 9 The photodegradation activity of N-doped TiO_2 catalysts under the UV light (a) and the all-wavelength light (b) illumination.

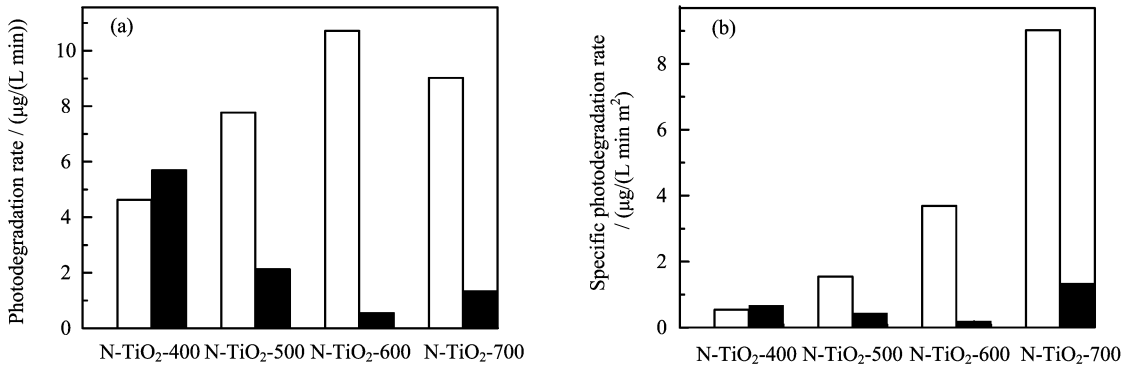

FIG. 10 The photodegradation rate (a) and the specific photodegradation rate (b) of methyl orange catalyzed by N-doped TiO_2 photocatalysts (white: UV-light and black: all-wavelength).

it remains unclear if the narrowing of band gap occurs for N-TiO_2-700.

The photocatalytic activity of various N-TiO_2 catalysts was evaluated by the photodegradation of methyl orange under both the UV light and all-wavelength light illuminations. The results are shown in Fig.9. When illuminated by the UV light lamp, all N-TiO_2 photocatalysts exhibit a certain photodegradation activity, in which N-TiO_2-600 shows the best performance (Fig.9(a)). However, when illuminated by the all-wavelength light, N-TiO_2-400 shows the best performance (Fig.9(b)). Figure 10 shows the specific photodegradation rate catalyzed by N-TiO_2 photocatalysts, illustrating the inherent photocatalytic activity of these photocatalysts. It can be seen that N-TiO_2-700 exhibit the highest specific photodegradation rate under both the UV light and the all-wavelength light illuminations, which indicates that the quantum yield of the photodegradation reaction is the highest in N-TiO_2-700. The quantum yield depends on several processes such as the excitation, bulk diffusion, and surface transfer of photoinduced charge-carriers in the photocatalysts. N-TiO_2-700 exhibits a more perfect crystallinity and thus fewer defects than other three photocatalysts, which could effectively inhibit the recombination of photoinduced charge-carriers. Recently it was reported that the anatase-rutile phase junctions on TiO_2 can effectively enhance the quantum yield of photocatalytic water splitting reaction to produce H_2 production process from water splitting [33]. N-TiO_2-700 is a mixture of anatase and rutile TiO_2 and the anatase-rutile phase junctions might also exist on N-TiO_2-700. Among anatase N-TiO_2-400, N-TiO_2-500, and N-TiO_2-600 photocatalysts, N-TiO_2-600 shows the highest specific photodegradation rate under the UV light illumination, which could be attributed to its perfect crystallinity; however, N-TiO_2-400 shows the highest specific photodegradation rate under the all-wavelength light illumination, which could be attributed to the narrowest band gap and thus the largest photon absorption capacity of N-TiO_2-400.

IV. CONCLUSION

We have successfully developed a novel approach for the synthesis of mesoporous N-doped TiO_2 by the controlled thermal decomposition of the molecular precursor ATO. The anatase-to-rutile phase transition occurs at 700 °C for N-doped TiO_2 photocatalysts. The doped

DOI:10.1088/1674-0068/23/01/95-101

N locates at the interstitial site of TiO_2 which leads to the narrowing of bad gap of pure anatase N-TiO_2. N-TiO_2-600 and N-TiO_2-400 exhibit the best performance in the photodegradation of methyl orange under the UV light and all-wavelength light illuminations, respectively; however, because of its perfect crystallinity and the existence of anatase-rutile phase junctions, N-TiO_2-700 exhibits the highest specific photodegradation rate, *i.e.*, the highest quantum yield, under both the UV light and all-wavelength light illuminations.

V. ACKNOWLEDGMENTS

This work was supported by the National Natural Science Foundation of China (No.20773113), the Solar Energy Project of Chinese Academy of Sciences, the Ministry of Education program for PCSIRT (No.IRT0756), and the Max Planck Gesellschaft of Chinese Academy of Sciences partner group.

[1] A. Salinaro, A. V. Emeline, J. Zhao, H. Hidaka, V. K. Ryabchunk, and N. Serpone, Pure Appl. Chem. **71**, 321 (1999).
[2] M. L. Sauer and D. F. Ollis, J. Catal. **163**, 215 (1996).
[3] K. Yamaguti and S. Sato, J. Chem. Soc. Faraday Trans. 1 **81**, 1237 (1985).
[4] R. Asahi, T. Morikawa, T. Ohwaki, K. Aoki, and Y. Taga, Science **293**, 169 (2001).
[5] T. Umebayashi, T. Yamaki, H. Itoh, and K. Asai, Appl. Phys. Lett. **81**, 454 (2002).
[6] J. C. Yu, J. Yu, W. Ho, Z. Jiang, and L. Zhang, Chem. Mater. **14**, 3808 (2002).
[7] W. Zhao, W. Ma, C. Chen, J. Zhao, and Z. Shuai, J. Am. Chem. Soc. **126**, 4782 (2004).
[8] G. Liu, Z. Chen, C. Dong, Y. Zhao, F. Li, G. Q. Lu, and H. M. Cheng, J. Phys. Chem. B **110**, 20823 (2006).
[9] S. Sakthivel and H. Kisch, Angew. Chem. Int. Ed. **42**, 4908 (2003).
[10] T. Lindgren, J. M. Mwabora, E. Avendaño, J. Jonsson, A. Hoel, C. G. Granqvist, and S. E. Lindquist, J. Phys. Chem. B **107**, 5709 (2003).
[11] Y. Nakano, T. Morikawa, T. Ohwaki, and Y. Taga, Appl. Phys. Lett. **86**, 132104 (2005).
[12] O. Diwald, T. L. Thompson, E. G. Goralski, S. D. Walck, and J. T. Yates Jr., J. Phys. Chem. B **108**, 52 (2004).
[13] M. Batzill, E. H. Morales, and U. Diebold, Phys. Rev. Lett. **96**, 026103 (2006).
[14] A. Ghicov, J. M. Macak, H. Tsuchiya, J. Kunze, V. Haeublein, L. Frey, and P. Schmuki, Nano Lett. **6**, 1080 (2006).
[15] D. Li and H. J. Haneda, J. Photochem. Photobiol. A **155**, 171 (2003).
[16] T. Ihara, M. Miyoshi, Y. Iriyama, O. Matsumoto, and S. Sugihara, Appl. Catal. B **42**, 403 (2003).
[17] S. Sakthivel, M. Janczarek, and H. Kisch, J. Phys. Chem. B **108**, 19384 (2004).
[18] C. D. Valentin, G. Pacchioni, A. Selloni, S. Livraghi, and E. Giamello, J. Phys. Chem. B **109**, 11414 (2005).
[19] S. K. Joung, T. Amemiya, M. Murabayashi, and K. Itoh, Appl. Catal. A **312**, 20 (2006).
[20] H. Irie, Y. Watanabe, and K. J. Hashimoto, J. Phys. Chem. B **107**, 5483 (2003).
[21] O. Diwald, T. L. Thompson, T. Zubkov, E. G. Goralski, S. D. Walck, and J. T. Yates Jr., J. Phys. Chem. B **108**, 6004 (2004).
[22] C. Burda, Y. Lou, X. Chen, A. C. S. Samia, J. Stout, and J. L. Gole, Nano Lett. **3**, 1049 (2003).
[23] T. Ihara, N. Miyoshi, Y. Iriyama, O. Matsumoto, and S. Sugihara, Appl. Catal. B **403**, 42 (2003).
[24] J. Fang, F. Wang, K. Qian, H. Z. Bao, Z. Q. Jiang, and W. X. Huang, J. Phys. Chem. C **112**, 18150 (2008).
[25] H. S. Potdar, S. B. Deshpande, A. S. Deshpande, Y. B. Khollam, A. J. Partil, S. D. Pradhan, and S. K. Date, Int. J. Inor. Mater **3**, 613 (2001).
[26] A. J. Partil, M. H. Shinde, H. S. Potdar, S. B. Deshpande, S. R. Sainkar, S. Mayadevi, and S. K. Date, Mater. Chem. Phys. **68**, 7 (2001).
[27] K. S. W. Sing, D. H. Everett, R. A. W. Haul, L. Moscou, R. A. Pierotti, J. Rouquerol, and T. Siemieniewska, Pure Appl. Chem. **57**, 603 (1985).
[28] J. F. Moulder, W. F. Stickle, P. E. Sobol, and K. D. Bomben, *Handbook of X-ray Photoelectron Spectroscopy*, Eden Prairie, MN: Perkin-Elmer Corporation, (1992).
[29] D. E. Gu, Y. Lu, B. C. Yang, and Y. D. Hu, Chem. Commun. 2453 (2008).
[30] N. C. Saha and H. G. Tompkins, J. Appl. Phys. **72**, 3072 (1992).
[31] X. Chen and C. Burda, J. Phys. Chem. B **108**, 15446 (2004).
[32] X. Chen, X. Wang, Y. Hou, J. Huang, L. Wu, and X. Fu, J. Catal. **255**, 59 (2008).
[33] J. Zhang, Q. Xu, Z. Feng, M. Li, and C. Li, Angew. Chem. Int. Ed. **47**, 1766 (2008).

DOI:10.1088/1674-0068/23/01/95-101